J Solid State Electrochem (2011) 15:2293–2304
DOI 10.1007/s10008-011-1459-8

ORIGINAL PAPER

A new method for electrocrystallization of $AgTCNQF_4$ and Ag_2TCNQF_4 ($TCNQF_4$ = 2,3,5,6-tetrafluoro-7,7,8,8-tetracyanoquinodimethane) in acetonitrile

Thanh H. Le · Anthony P. O'Mullane · Lisandra L. Martin · Alan M. Bond

Received: 26 April 2011 / Accepted: 2 June 2011 / Published online: 12 July 2011

Abstract Semiconducting $AgTCNQF_4$ ($TCNQF_4$=2,3,5,6-tetrafluoro-7,7,8,8-tetracyanoquinodimethane) has been electrocrystallized from an acetonitrile (0.1 M Bu_4NPF_6) solution containing $TCNQF_4$ and $Ag(MeCN)_4^+$. Reduction of $TCNQF_4$ to the $TCNQF_4^{1-}$ anion, followed by reaction with $Ag(MeCN)_4^+$ forms crystalline $AgTCNQF_4$ on the electrode surface. Electrochemical synthesis is simplified by the reduction of $TCNQF_4$ prior to $Ag(MeCN)_4^+$ compared with the analogous reaction of the parent TCNQ to form AgTCNQ, where these two processes are coincident. Cyclic voltammetry and surface plasmon resonance studies reveal that the electrocrystallization process is slow on the voltammetric time scale (scan rate=20 mV s^{-1}) for $AgTCNQF_4$, as it requires its solubility product to be exceeded. The solubility of $AgTCNQF_4$ is higher in the presence of 0.1 M Bu_4NPF_6 supporting electrolyte than in pure solvent. Cyclic voltammetry illustrates a dependence of the reduction peak potential of $Ag(MeCN)_4^+$ to metallic Ag on the electrode material with the ease of reduction following the order Au<Pt<GC<ITO. Ultraviolet-visible, Fourier transform infrared, and Raman spectra confirmed the formation of reduced $TCNQF_4^{1-}$ and optical microscopy showed needle-shaped morphology for the electrocrystallized $AgTCNQF_4$. $AgTCNQF_4$ also can be formed by solid–solid transformation at a $TCNQF_4$-modified electrode in contact with aqueous media containing Ag^+ ions. Chemically and electrochemically synthesized $AgTCNQF_4$ are spectroscopically identical. Electrocrystallization of Ag_2TCNQF_4 was also investigated; however, this was found to be thermodynamically unstable and readily decomposed to form $AgTCNQF_4$ and metallic Ag, as does chemically synthesized Ag_2TCNQF_4.

Keywords $AgTCNQF_4$ · Ag_2TCNQF_4 · Electrocrystallization

T. H. Le · L. L. Martin (✉) · A. M. Bond (✉)
School of Chemistry, Monash University,
Clayton, VIC 3800, Australia
e-mail: Lisa.Martin@monash.edu

A. M. Bond
e-mail: Alan.Bond@monash.edu

A. P. O'Mullane
School of Applied Sciences, RMIT University,
GPO Box 2476 V, Melbourne, VIC 3001, Australia

Introduction

Metal-organic charge-transfer (CT) complexes based on TCNQ (7,7,8,8-tetracyanoquinodimethane) have been intensively studied due to their novel conducting and/or magnetic properties [1–4]. TCNQ-based materials have been used for data storage [5, 6], in catalysis [7–9], and in magnetic and sensor devices [10, 11]. In contrast, investigation of $TCNQF_4$-based CT complexes ($TCNQF_4$= 2,3,5,6-tetrafluoro-7,7,8,8-tetracyanoquinodimethane) are much more limited, although some materials have been synthesized and characterized [12–19]. One of these is $AgTCNQF_4$, a metal-organic CT semiconducting material [16] which is regarded as an excellent candidate for field-emission cathodes [17], reversible bi-stable electrical and optical switches, as well as memory storage [16]. The chemical synthesis of $AgTCNQF_4$ has been reported by mixing the Ag^+ cation and the $TCNQF_4^{1-}$ radical anion in acetonitrile [13], spontaneous redox reaction by placing Ag foil in a dry and degassed acetonitrile solution containing saturated $TCNQF_4$, and then heating to about 90 °C to achieve a film of $AgTCNQF_4$ on the Ag substrate [20]. Alternatively, a solid-phase reaction between $TCNQF_4$

powder and Ag metal is possible by precisely controlling the temperature and time [16, 17]. $AgTCNQF_4$ also has been electrochemically synthesized by slow reduction of $TCNQF_4$ at an Ag electrode with a constant current in a two-compartment cell configuration containing acetonitrile [13]. The single-crystal X-ray structure of the electrocrystallized $AgTCNQF_4$ has been determined and is not isostructural with AgTCNQ [13]. The silver cations have a pseudotetraheadral geometry and the $TCNQF_4^{1-}$ anions are nearly perfectly eclipsed and exhibit a high degree of dimerization, which results in the compound being essentially diamagnetic [13]. Ag_2TCNQF_4 also has been chemically synthesized by direct reaction of thin films of $TCNQF_4$ and Ag at 100 °C for approximately 100 s, where it was found to photodecompose to $AgTCNQF_4$ and metallic Ag [12].

In this paper, a potentiostatic electrochemical method for synthesizing $AgTCNQF_4$ and Ag_2TCNQF_4 in acetonitrile is reported. Thus, $AgTCNQF_4$ and Ag_2TCNQF_4 were electrocrystallized onto the surface of an inert electrode by sequential reduction of $TCNQF_4$ to $TCNQF_4^{1-}$ and then to $TCNQF_4^{2-}$ in acetonitrile (0.1 M Bu_4NPF_6), followed by combination with $Ag(MeCN)_4^+$ also present in the solution to form $AgTCNQF_4$ and Ag_2TCNQF_4, respectively. Factors potentially affecting the electrochemical synthesis, such as the concentrations of $TCNQF_4$ and $Ag(MeCN)_4^+$, scan rate, and electrode material have been explored. The isolated electrocrystallized $AgTCNQF_4$ complex was characterized by a range of microscopic and spectroscopic techniques, and in situ by surface plasmon resonance (SPR). Electrochemical synthesis of bulk Ag_2TCNQF_4 is complicated by the close proximately of the $TCNQF_4^{1-/2-}$ process and the reduction of $Ag(MeCN)_4^+$ to Ag metal. The solubility and solubility product of $AgTCNQF_4$ in acetonitrile with and without 0.1 M Bu_4NPF_6 supporting electrolyte also have been determined, but efforts to determine the solubility of Ag_2TCNQF_4 have not been successful because of thermodynamic instability, in which Ag_2TCNQF_4 undergoes an internal redox reaction to generate $AgTCNQF_4$ (as detected by UV-vis and FTIR spectroscopy) and metallic Ag.

Materials and methods

Chemicals

$Ag(MeCN)_4BF_4$ (98%, Aldrich), $AgNO_3$ (99.998%, Aldrich), $TCNQF_4$ (97%, Aldrich), acetonitrile (HPLC grade, Omnisolv), acetone (Suprasolv, Merck KGaA), and isopropanol (BDH) were used as received from the manufacturers. Bu_4NPF_6 (Aldrich) was recrystallized twice from 96% ethanol (Merck) and then dried at 100 °C under vacuum for 24 h.

Electrochemisty

Voltammetric measurements were carried out at room temperature (22±2 °C) with a Bioanalytical Systems (BAS) 100W electrochemical workstation and a standard three-electrode cell configuration. Working electrodes (WEs) were 3.0-mm diameter glassy carbon (GC) (BAS), gold or platinum (1.6-mm diameter, BAS) disks, or indium tin oxide (ITO)-coated glass plates (0.1–0.2 cm^2) with a resistance of 10 Ω/sq (as quoted by the manufacturer, Prazisions Glas and Optik GmbH). All working electrodes, except for ITO, were polished with 0.3 μm alumina slurry on Microcloth polishing cloth, washed with deionized water (purified from a Millipore system, resistivity of 18.2 MΩ cm) and then sonicated in an ultrasonic bath for 5 min. ITO electrodes were cleaned by sonication in isopropanol and acetone for 5 and 10 min, respectively, and then washed with deionized water and dried under a stream of nitrogen gas. A silver wire placed in an acetonitrile solution containing 1.0 mM $AgNO_3$ and 0.1 M Bu_4NPF_6 was used to form an Ag/Ag^+ reference electrode (RE) (the potential of this RE is −0.14 V versus the ferrocene/ferrocenium ($Fc^{0/+}$) couple). The counter electrode (CE) was platinum wire (1.0-mm diameter). In the case of rotating disk electrode (RDE) experiments, the Ag/Ag^+ and Pt wire mentioned above also were used as reference and counter electrodes, while the working electrode was a 3.0-mm diameter GC electrode attached to BAS RDE-2 RDE assembly. In case of solid–solid state transformation experiments, $TCNQF_4$ crystals, physically adhered to GC and ITO electrode surfaces, were used as the working electrodes, the reference electrode was aqueous Ag/AgCl (3.0 M KCl) (BAS) and Pt wire (1.0-mm diameter) was used as the counter electrode. In bulk electrolysis experiments, a three-compartment cell was used with each of the working (Pt foil), reference (Ag/Ag^+), and counter (Pt mesh) electrodes placed in one compartment of the cell. Stirring via a magnetic bar in the working electrode compartment was used during the course of bulk electrolysis. These bulk electrolysis experiments were stopped when the current decreased to 0.1% of the initial value. Nitrogen gas was used to purge solutions of oxygen prior to commencing electrochemical experiments. A stream of this gas was maintained above the solution during the course of the experiments.

In situ SPR experiments were carried out using an AutoLab ESPRIT system, interfaced to an AutoLab PGSTAT100 potentiostat. A 50-nm thick gold film coated on a glass plate was used as both the SPR substrate and working electrode (all instrumentations and electrodes for SPR experiments were supplied by ECO-Chemie). The angle of the minimum reflection in the Kretschmann configuration [21] was used to examine the SPR response

during the course of electrochemical experiments. Platinum wires were used as quasi-reference and counter electrodes in the SPR-electrochemical measurements.

Other instrumentation

UV-vis spectra were recorded with a Varian Cary 5000 UV-vis NIR spectrophotometer on solutions contained in a 1.0-cm path length cuvette. FTIR spectra were obtained with a Varian UMA600 IR microscope and FTS7000 optics bench using 128 scans and a resolution of 8 cm^{-1}. A Renishaw Invia Raman spectrograph, using an Argon ion laser excitation at 633 nm, was used to measure Raman spectra. Optical microscopic images were collected with an Olympus BX51M optical microscope at a magnification factor of 20. SEM image was recorded with a FEI Nova SEM instrument.

Results and discussion

Solubility of $AgTCNQF_4$ in acetonitrile

A 10.0 mM $TCNQF_4^{1-}$ solution was prepared by exhaustive reductive electrolysis of 5.0 mL of 10.0 mM $TCNQF_4$ acetonitrile solution (0.1 M Bu_4NPF_6) with the potential of the Pt working electrode held at 100 mV vs. Ag/Ag^+ (all potentials in this paper are reported versus $Ag/AgNO_3$ (1.0 mM) in acetonitrile containing 0.1 M Bu_4NPF_6 unless otherwise stated). 1.0 mL of 100 mM $Ag(MeCN)_4^+$ acetonitrile solution was then added into the $TCNQF_4^{1-}$ solution with stirring for 1 min. A dark blue precipitate formed immediately and was collected after centrifugation and the solid was washed three times with 1.0 mL of acetonitrile to ensure removal of excess $Ag(MeCN)_4^+$ and Bu_4NPF_6 supporting electrolyte. Finally, 2.0 mL of acetonitrile was added into the test tube containing pure solid $AgTCNQF_4$, followed by sonication for 5 min to achieve good mixing with the dissolved material. The $AgTCNQF_4$ saturated acetonitrile solution and solid $AgTCNQF_4$ were separated by centrifugation and filtration. The solid $AgTCNQF_4$ was placed on an ITO surface and dried under vacuum prior to characterization by spectroscopic and microscopic techniques (see section "Chemically synthesized $AgTCNQF_4$"). The concentration of the $TCNQF_4^{1-}$ remaining in the saturated solution was determined by UV-vis spectroscopy and measuring the absorbance at 411 nm and subsequent reference to a calibration curve, and found to be $7.08\pm0.16\times10^{-4}$ M. Consequently, the values for the solubility and solubility product of $AgTCNQF_4$ in acetonitrile are $7.08\pm0.16\times10^{-4}$ M and $5.01\pm0.22\times10^{-7}$ M^2, respectively.

RDE voltammetry also was used to determine the concentration of $TCNQF_4^{1-}$. $TCNQF_4^{1-}$ is oxidized to neutral $TCNQF_4$ (Eq. 1) in acetonitrile (0.1 M Bu_4NPF_6) under RDE conditions to give a limiting current that is proportional to the concentration of $TCNQF_4^{1-}$. Solid Bu_4NPF_6 was added to a saturated acetonitrile solution of $AgTCNQF_4$ to give the 0.1 M electrolyte concentration needed for RDE experiments. A 3.0-mm diameter GC RDE was used at a rotation rate of 1,000 rpm and scan rate of 10 mV s^{-1}, and gave well-defined limiting currents (see Fig. 1) for the three processes given in Eqs. 1 to 3. The solubility and solubility product values were found to be the same as determined by UV-vis spectroscopy.

$$TCNQF_{4(MeCN)}^{1-} \rightleftharpoons TCNQF_{4(MeCN)} + e^- \quad (1)$$

$$TCNQF_{4(MeCN)}^{1-} + e^- \rightleftharpoons TCNQF_4{}^{2-}{}_{(MeCN)} \quad (2)$$

$$Ag^+{}_{(MeCN)} + e^- \rightleftharpoons Ag_{(s)} \quad (3)$$

The solubility of $AgTCNQF_4$ was then re-determined in an acetonitrile solution containing 0.1 M Bu_4NPF_6 electrolyte. In this case, 2.0 mL of acetonitrile containing 0.1 M Bu_4NPF_6 was used for RDE and UV-vis methods and the concentration of $TCNQF_4^{1-}$ in the saturated solution was determined to be $1.10\pm0.04\times10^{-3}$ M. This value translates to a solubility product for $AgTCNQF_4$ of $1.22\pm0.08\times10^{-6}$ M^2, indicating that the solubility of $AgTCNQF_4$ in the presence of 0.1 M Bu_4NPF_6 is higher than that in neat solvent. This enhancement in solubility also has been observed for AgTCNQ and CuTCNQ [22, 23] in the presence of electrolyte and, in this case, can be attributed to the ion pairing of $Ag(MeCN)_4^+$ with PF_6^- and $TCNQF_4^{1-}$ with Bu_4N^+, which favors the dissociation of $AgTCNQF_4$ to $Ag(MeCN)_4^+$ and $TCNQF_4^{1-}$ [22].

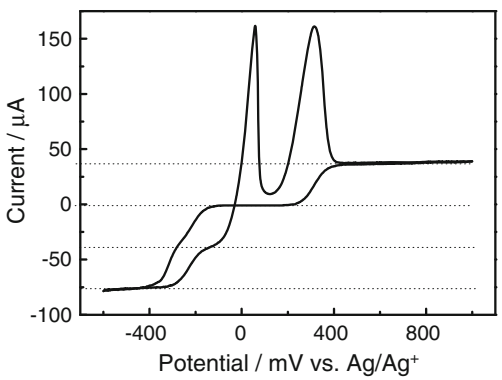

Fig. 1 Cyclic voltammogram obtained with a 3.0-mm diameter GC electrode RDE (1,000 rpm, 10 mV s^{-1}) for $AgTCNQF_4$ dissolved in acetonitrile (0.1 M Bu_4NPF_6)

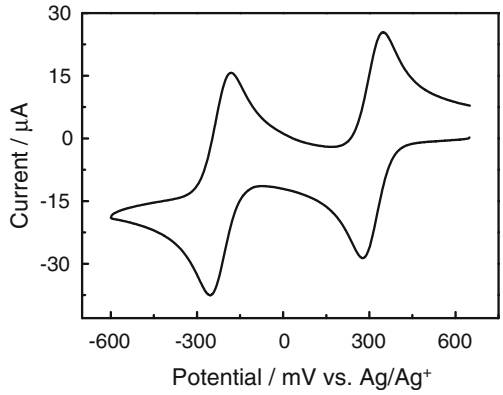

Fig. 2 Cyclic voltammogram obtained with a 3.0-mm diameter GC electrode at a scan rate of 100 mV s^{-1} for 1.0 mM $TCNQF_4$ in acetonitrile (0.1 M Bu_4NPF_6)

Cyclic voltammetric study of the electrocrystallization of $AgTCNQF_4$ and Ag_2TCNQF_4 in acetonitrile

Voltammetry of $TCNQF_4$ and $Ag(MeCN)_4^+$ in acetonitrile (0.1 M Bu_4NPF_6) solution

The limited solubility of $AgTCNQF_4$ in acetonitrile (0.1 M Bu_4NPF_6) indicated that electrocrystallization of $AgTCNQF_4$ should be possible. A cyclic voltammogram of 1.0 mM $TCNQF_4$ in acetonitrile (0.1 M Bu_4NPF_6) using a GC electrode recorded at a scan rate of 100 mV s^{-1} is shown in Fig. 2. $TCNQF_4$ underwent the two chemically and electrochemically reversible one-electron reduction processes (reverse of Eq. 1 and Eq. 2) as expected [24]. The mid-point potentials E_m for these processes at GC, Au, Pt, and ITO electrodes are given in Table 1 (where $E_m{}^1 = (E_{p1}{}^{red}+E_{p1}{}^{ox})/2$ and $E_m{}^2=(E_{p2}{}^{red}+E_{p2}{}^{ox})/2$, and $E_p{}^{red}$ and $E_p{}^{ox}$ are reduction and oxidation peak potentials, respectively, for processes related to Eqs. 1 and 2). E_m, as expected, is almost independent of electrode material.

Cyclic voltammograms for 2.0 mM $Ag(MeCN)_4^+$ in acetonitrile (0.1 M Bu_4NPF_6) are shown in Fig. 3. In the case of reduction of $Ag(MeCN)_4^+$ to Ag metal, the process is strongly dependent on the nature of the electrode material. Thus, $Ag(MeCN)_4^+$ cations follow the ease of reduction order, Au<Pt<GC<ITO (Fig. 3e). Moreover, $E_p{}^{red}$ for reduction of $Ag(MeCN)_4^+$ in the first cycle of potential is always more negative than in subsequent cycles. For example, at a GC electrode in the first cycle with a scan rate of 100 mV s^{-1}, $E_p{}^{red}$ for the reduction of $Ag(MeCN)_4^+$ to metallic Ag is at −331 mV, whereas in the second cycle, $E_p{}^{red}$ is −140 mV. Additionally, a sharp oxidation peak for stripping silver occurs at 68 mV and current crossover is detected at −260 and −77 mV in the first cycle. These results imply that the reduction of $Ag(MeCN)_4^+$ to Ag metal occurs via a nucleation and growth process [23]. A comparison with TCNQ shows the reduction to $TCNQ^{1-}$ occurs at a potential value slightly more positive than for $Ag(MeCN)_4^+$ reduction [23]. For $TCNQF_4$, the first reduction process is now well removed from that of $Ag(MeCN)_4^+$ (compare Figs. 2 and 3). Consequently, $AgTCNQF_4$ can be readily electrosynthesized via scheme 1. However, in principle, Ag_2TCNQF_4 cannot be electrochemically synthesized at Au or Pt electrodes where $Ag(MeCN)_4^+$ is reduced prior to the $TCNQF_4{}^{1-/2-}$ process, although at GC or ITO electrodes, this is now possible (via scheme 2) because the reduction of $TCNQF_4{}^{1-}$ to $TCNQF_4{}^{2-}$ is slightly more positive than that of $Ag(MeCN)_4^+$. However, efforts to achieve electrochemical synthesis of bulk Ag_2TCNQF_4 on GC and ITO have not been successful as the potentials for reduction of $TCNQF_4{}^{1-}$ and $Ag(MeCN)_4^+$ on GC and ITO are still very close. Furthermore, Ag_2TCNQF_4 is not a stable species in acetonitrile (see section "Chemically synthesized Ag_2TCNQF_4").

Scheme 1

$$TCNQF_{4(MeCN)} + e^- \rightleftharpoons TCNQF_4{}^{1-}_{(MeCN)} \quad (4a)$$

$$Ag^+{}_{(MeCN)} + TCNQF_4{}^{1-}_{(MeCN)} \rightleftharpoons AgTCNQF_{4(s)} \quad (4b)$$

Scheme 2

$$TCNQF_4{}^{1-}_{(MeCN)} + e^- \rightleftharpoons TCNQF_4{}^{2-}_{(MeCN)} \quad (5a)$$

$$TCNQF_4{}^{2-}_{(MeCN)} + 2Ag^+{}_{(MeCN)} \rightleftharpoons Ag_2TCNQF_{4(s)} \quad (5b)$$

Table 1 Summary of voltammetric data obtained at a scan rate of 100 mV s^{-1} for $TCNQF_4$ and $Ag(MeCN)_4^+$ in acetonitrile (0.1 M Bu_4NPF_6) with GC, Au, Pt, and ITO electrodes (potential (millivolts) vs. Ag/Ag^+)

WE	Compound										
	$TCNQF_4$							$Ag(MeCN)_4^+$ (1st cycle)			
	$E_p{}^{red1}$	$E_p{}^{ox1}$	$E_m{}^1$	$E_p{}^{red2}$	$E_p{}^{ox2}$	$E_m{}^2$	ΔE^0	$E_p{}^{red}$	$E_p{}^{ox}$	E_m	ΔE_p
GC	277	345	311	−255	−185	−220	531	−331	68	−132	399
Au	277	343	310	−255	−185	−220	530	−99	79	−10	178
Pt	277	343	310	−256	−186	−221	531	−133	59	−37	192
ITO	201	406	304	−335	−157	−246	550	−447	34	−207	481

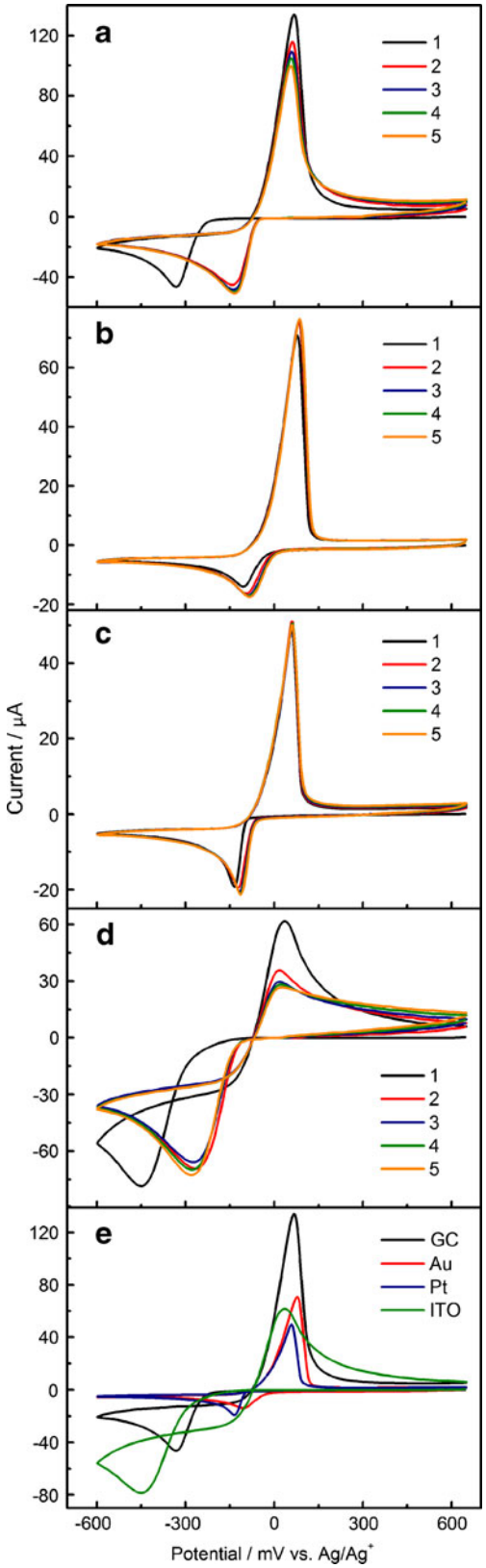

Fig. 3 Cyclic voltammograms obtained at a scan rate of 100 mV s^{-1} at GC, Au, Pt, ITO electrodes for 2.0 mM $Ag(MeCN)_4^+$ in acetonitrile (0.1 M Bu_4NPF_6) **a**–**d** represent number of cycles across potential range at GC, Au, Pt, ITO, **e** first cycle for each electrode

Cyclic voltammetry of $TCNQF_4$ in the presence of $Ag(MeCN)_4^+$ in acetonitrile (0.1 M Bu_4NPF_6)

1. Reduction of $TCNQF_4$ to $TCNQF_4^{1-}$ in the presence of $Ag(MeCN)_4^+$

   In order to ensure electrocrystallization of $AgTCNQF_4$ rather than Ag_2TCNQF_4 occurs, the potential was switched at 50 mV, which lies between the $TCNQF_4^{0/1-}$ and $TCNQF_4^{1-/2-}$ processes. The concentration ratios of $TCNQF_4$ and $Ag(MeCN)_4^+$ were varied to produce the cyclic voltammetric behavior exhibited in Fig. 4a, b and c. Clearly, when the $Ag(MeCN)_4^+$ concentration is constant and that of $TCNQF_4$ is increased, the ratio of oxidation and reduction peak current (i_p^{ox}/i_p^{red}) decreases, which is expected if reduction of $TCNQF_4$ to $TCNQF_4^{1-}$ is followed by electrocrystallization of $AgTCNQF_4$ (scheme 1) [25]. However, electrocrystallization can only occur when the solubility product of $AgTCNQF_4$ is exceeded at the electrode surface and if the rate of precipitation is sufficiently fast. Studies with 2.0 mM $TCNQF_4$ and 100 mM $Ag(MeCN)_4^+$ in acetonitrile (0.1 M Bu_4NPF_6) solution show that the precipitation kinetics are relatively slow as the i_p^{ox}/i_p^{red} ratio approaches unity at high scan rate of >2 V s^{-1} (data not shown). Interestingly, no well-defined stripping peak was found when the potential was scanned in the positive direction to very positive potentials under conditions relevant to Fig. 4c. This behavior implies that $AgTCNQF_4$ either does not precipitate on the time scale of cyclic voltammetry or predominantly precipitates away from the surface of the electrode (under conditions of Fig. 4c, a dark blue precipitate is observed in the solution if a potential of 150 mV is applied for 15 min). However, when a solution of 2.0 mM $TCNQF_4$ and 100 mM $Ag(MeCN)_4^+$ is used, a broad oxidation stripping process is detected at around 770 mV on the reverse scan (Fig. 4d), implying that $AgTCNQF_4$ is now electrocrystallized onto the electrode surface and oxidized back to neutral $TCNQF_4$.
2. Reduction of $TCNQF_4^{1-}$ to $TCNQF_4^{2-}$ in the presence of $Ag(MeCN)_4^+$

   When the switching potential was set at −170 mV, and hence slightly more negative than the onset of the $TCNQF_4^{1-/2-}$ process, with 1.0 mM $TCNQF_4$ and 10.0 mM $Ag(MeCN)_4^+$ present, the cyclic voltammograms at a GC electrode become much more complicated. On the first scan in the negative potential direction, the $TCNQF_4^{0/1-}$ reduction process is still located at its normal position; in contrast, the second $TCNQF_4^{1-/2-}$ process is modified and now found at −147 mV. On reversing the scan direction, a sharp stripping oxidation process at 215 mV is followed by the $TCNQF_4^{1-}$/

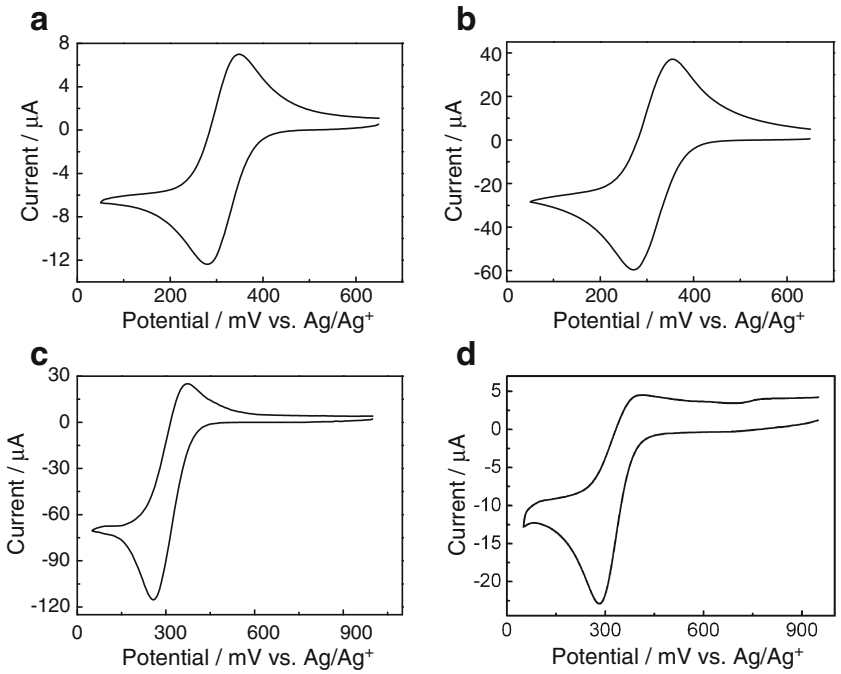

Fig. 4 Cyclic voltammograms obtained at a scan rate of 20 mV s^{-1} with a 3.0-mm diameter GC electrode in acetonitrile (0.1 M Bu_4NPF_6) containing **a**–**c** 10.0 mM $Ag(MeCN)_4^+$ and 1.0, 5.0, 10.0 mM $TCNQF_4$, respectively, **d** 100 mM $Ag(MeCN)_4^+$ and 2.0 mM $TCNQF_4$

$TCNQF_4$ process (Fig. 5a, black curve). The new oxidation process is assumed to be associated with stripping of electrocrystallized solid Ag_2TCNQF_4, which was formed via scheme 2. When the potential was switched at the more negative value of −200 mV, on scanning in the positive potential direction, a current loop and a sharp stripping process at 50 mV were detected (Fig. 5a, red curve) in addition to the Ag_2TCNQF_4 stripping process. The current loop is due to the nucleation and growth of metallic Ag on the GC electrode surface [26–28] (Eq. 3). In the reverse potential scan direction, a broad oxidation process also is detected at around 450 mV. This process is presumed to result from the oxidation of $AgTCNQF_4$, which is formed by the oxidation of $TCNQF_4^{2-}$ in Ag_2TCNQF_4 back to $TCNQF_4^{1-}$, followed by reaction in Eq. 4b. However, the potential for the oxidation process is less positive than that of ~770 mV that is detected when the potential is switched at 50 mV (Fig. 4d). Therefore, $AgTCNQF_4$ derived from the oxidation of Ag_2TCNQF_4 rather than from combination of $Ag(MeCN)_4^+$ and $TCNQF_4^{1-}$ in the negative potential direction scan may exist in a different phase. Interestingly, two AgTCNQ oxidation processes also were seen in the cyclic voltammetry in acetonitrile solutions containing TCNQ and $Ag(MeCN)_4^+$ [23].

The deposition of Ag_2TCNQF_4 and Ag onto the electrode surface was confirmed by cyclic voltammetric experiments using a RDE. Figure 5b shows GC RDE voltammograms in acetonitrile (0.1 M Bu_4NPF_6) containing 1.0 mM $TCNQF_4$ with 1.0 mM $Ag(MeCN)_4^+$. When scanning the potential in the negative direction, reduction of $TCNQF_4$ to $TCNQF_4^{1-}$ and then $TCNQF_4^{2-}$ is followed by reduction of $Ag(MeCN)_4^+$

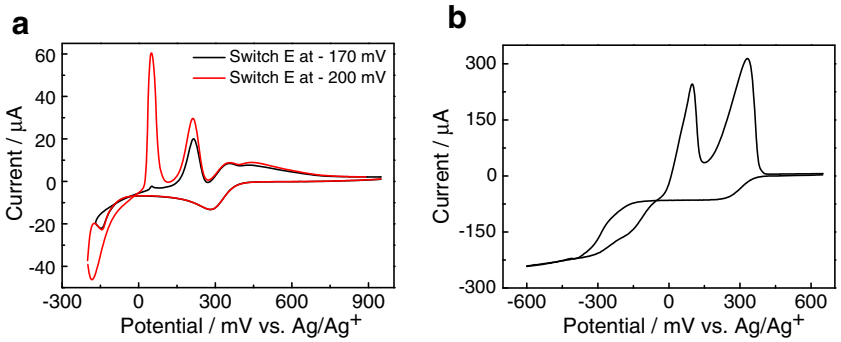

Fig. 5 Cyclic voltammograms obtained in acetonitrile (0.1 M Bu_4NPF_6) with **a** a 3.0-mm diameter GC electrode at a scan rate of 20 mV s^{-1} for 1.0 mM $TCNQF_4$ and 10.0 mM $Ag(MeCN)_4^+$, **b** a 3.0-mm diameter GC RDE (1,000 rpm, 10 mV s^{-1}) for 1.0 mM $TCNQF_4$ and 1.0 mM $Ag(MeCN)_4^+$

to metallic silver. On reversing the scan direction, stripping of Ag and Ag_2TCNQF_4 formed at the surface occurs when the potential was scanned in the positive direction.

The electrocrystallization and stripping of Ag_2TCNQF_4 were also explored as a function of scan rate and other parameters. Cyclic voltammograms in Fig. 6a reveal that for 1.0 mM $TCNQF_4$ and 2.0 mM $Ag(MeCN)_4^+$ at a GC electrode (scan rate=20 mV s^{-1}, potential range +650 to −600 mV), reduction of $TCNQF_4^{1-}$ occurs just prior to that of $Ag(MeCN)_4^+$ in the first cycle, but in later cycles of potential, both processes are almost coincident. This change is expected on the basis of the voltammetry of $Ag(MeCN)_4^+$ (Fig. 3a). However, the potentials for stripping of Ag and Ag_2TCNQF_4 do not change upon cycling the potential. Besides Ag and Ag_2TCNQF_4 stripping, only one other oxidation process at −200 mV is observed, which corresponds to the oxidation of $TCNQF_4^{2-}{}_{(MeCN)}$ to $TCNQF_4^{1-}{}_{(MeCN)}$ (Fig. 6a dark yellow curve).

In another series of experiments with 1.0 mM $TCNQF_4$ and 2.0 mM $Ag(MeCN)_4^+$, the magnitude of the Ag_2TCNQF_4 stripping peak was investigated as a function of electrocrystallization time. In this case, the potential was set at −170 mV for a certain time before sweeping the potential in the positive direction. Under these conditions, the peak current at 230 mV for stripping Ag_2TCNQF_4 from the electrode increases with deposition time (Fig. 6b). In contrast, increasing the scan rate under cyclic voltammetric conditions decreases the oxidation of Ag_2TCNQF_4 (Fig. 6c), which implies that its deposition onto the electrode surface also is kinetically controlled.

Role of working electrode material

Cyclic voltammograms for 1.0 mM $TCNQF_4$ and 2.0 mM $Ag(MeCN)_4^+$ in acetonitrile (0.1 M Bu_4NPF_6) at GC, Au, Pt, and ITO electrodes are shown in Fig. 7. Since the reduction of $Ag(MeCN)_4^+$ to Ag on Au electrode occurs prior to that for the reduction of $TCNQF_4^{1-}$ to $TCNQF_4^{2-}$ by about 200 mV, Ag_2TCNQF_4 cannot be formed, as indicated in scheme 2. Hence, no Ag_2TCNQF_4 stripping process was detected in the positive potential scans at the Au electrode (Fig. 7b). In contrast, Ag_2TCNQF_4 can be electrocrystallized directly onto GC, Pt, and ITO electrodes as Ag_2TCNQF_4 stripping process is observed when scanning the potential in the positive direction (Fig. 7a, c, d), even though the reduction of $Ag(MeCN)_4^+$ cations occurs slightly before that of the $TCNQF_4^{1-}$ at the Pt electrode. Since the reduction of $TCNQF_4^{1-}$ occurs slightly before that of $Ag(MeCN)_4^+$ at GC and ITO electrodes, these electrode materials are preferable for electrochemical synthesis of Ag_2TCNQF_4.

The influence of $Ag(MeCN)_4^+$ concentration on the formation of Ag_2TCNQF_4

Voltammograms derived from 1.0 mM $TCNQF_4$ (Fig. 8) reveal that the second $TCNQF_4^{1-}$ reduction peak potential (E_p^{Red2}) depends markedly on the $Ag(MeCN)_4^+$ concentration. In contrast, the peak potential for the first $TCNQF_4$ to $TCNQF_4^{1-}$ reduction (E_p^{Red1}) is independent of the $Ag(MeCN)_4^+$ concentration. E_p^{Red2} shifted 78 mV to more positive potential when $Ag(MeCN)_4^+$ concentration was increased from 0.0 to 10.0 mM. The shift of E_p^{Red2} to more positive potential is consistent with the combination of $TCNQF_4^{2-}$ and $Ag(MeCN)_4^+$ [25].

The influence of scan rate

Peak potentials E_p^{Red1}, E_p^{Red2}, and E_p^{Red3} shift 15, 15, and 181 mV, respectively, to more negative potential when the scan rate is increased from 20 to 500 mV s^{-1} at a GC electrode under conditions described in Fig. 9. Thus, although a small IR_u drop may be present, the scan rate does not significantly affect the first and second reduction peak potentials (E_p^{Red1} and E_p^{Red2}). In contrast, E_p^{Red3}

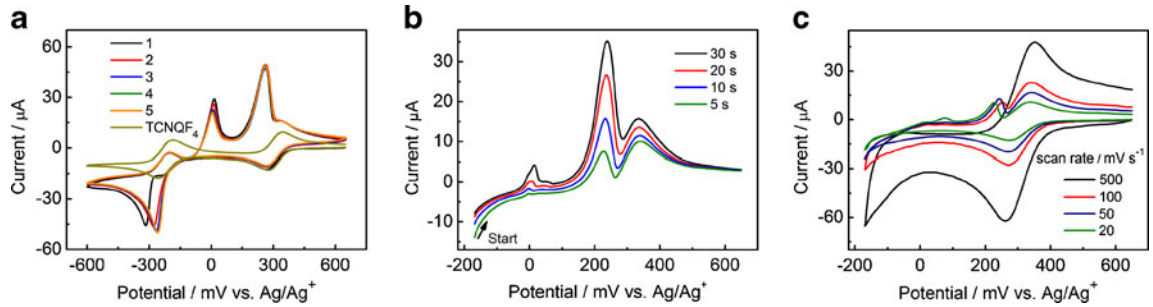

Fig. 6 Voltammograms obtained in acetonitrile (0.1 M Bu_4NPF_6) with a 3.0-mm diameter GC electrode **a** cyclic voltammetry at a scan rate of 20 mV s^{-1} for 1.0 mM $TCNQF_4$ and 2.0 mM $Ag(MeCN)_4^+$ (First five cycles of potential compared to 1.0 mM $TCNQF_4$), **b** solution as in **a** but potential held at −170 mV for designated times before sweeping the potential to 650 mV (scan rate=20 mV s^{-1}), **c** cyclic voltammetry for 1.0 mM $TCNQF_4$ and 5.0 mM $Ag(MeCN)_4^+$ at designated scan rates

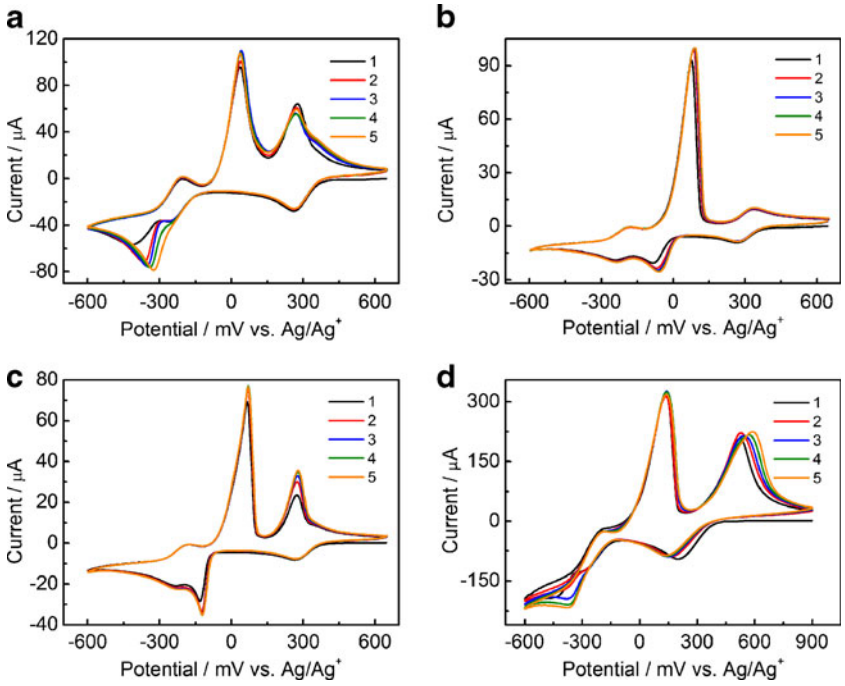

Fig. 7 Cyclic voltammograms (first five cycles of potential) for 1.0 mM $TCNQF_4$ and 2.0 mM $Ag(MeCN)_4^+$ in acetonitrile (0.1 M Bu_4NPF_6) using **a** GC, **b** Au, **c** Pt, and **d** ITO electrode at a scan rate of 100 mV s^{-1}

attributed to the reduction of $Ag(MeCN)_4^+$ to Ag metal is strongly dependent on scan rate as expected for a nucleation and growth mechanism [26, 27].

Surface plasmon resonance study

In situ cyclic voltammetric and SPR experiments on gold-coated glass electrodes have been used to monitor mass change due to deposition onto or stripping from an electrode surface [21, 23], although caution is needed in the interpretation of these data since the changes in the solution near the electrode surface also may affect the SPR intensity [21]. SPR monitoring of cyclic voltammograms in acetonitrile (0.1 M Bu_4NPF_6) containing either 1.0 mM $TCNQF_4$ and 2.0 mM $Ag(MeCN)_4^+$, or 10.0 mM $TCNQF_4$ and 10.0 mM $Ag(MeCN)_4^+$ is shown in Fig. 10. Clearly, no evidence for $AgTCNQF_4$ deposition on the gold electrode surface is found when the potential was switched prior to the reduction of $TCNQF_4^{1-}$ to $TCNQF_4^{2-}$ (compare Fig. 10a with c, and e with f) because the SPR behaviors for mixtures of $TCNQF_4$ and $Ag(MeCN)_4^+$ are very similar to those found for solutions containing only $TCNQF_4$. Interestingly, the i_p^{ox} value for the mixture of 10.0 mM $TCNQF_4$ and 10.0 mM $Ag(MeCN)_4^+$ is less than that for pure 10.0 mM $TCNQF_4$ (170 vs. 230 μA from baseline), while i_p^{red} values are the same (255 μA). This implies that $TCNQF_4^{1-}$ has reacted with $Ag(MeCN)_4^+$ to form $AgTCNQF_4$ near to the electrode surface, but the solid has not adhered to the electrode surface. In contrast, when the potential range was extended to more negative values, a large change in the SPR signal accompanied the deposition and stripping of metallic Ag. The cyclic voltammetric and SPR response in these experiments are consistent with data derived from a 1.6-mm diameter Au disk electrode (Fig. 7b). That is, Ag deposition occurs before reduction of the $TCNQF_4^{1-}$ to the $TCNQF_4^{2-}$.

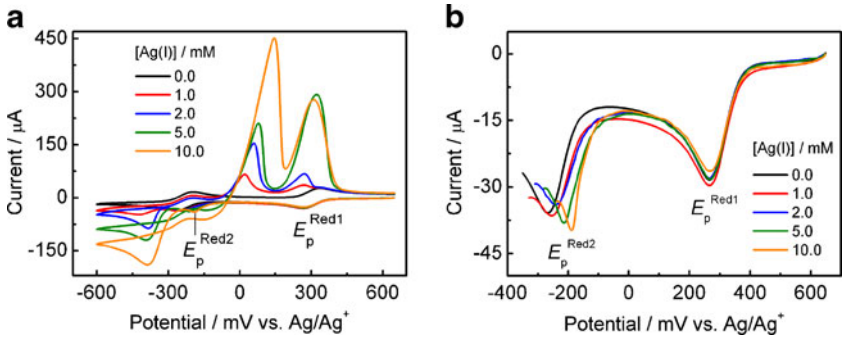

Fig. 8 **a** Cyclic voltammograms obtained in acetonitrile (0.1 M Bu_4NPF_6) with a 3.0-mm diameter GC electrode (scan rate= 100 mV s^{-1}) for 1.0 mM $TCNQF_4$ and designated concentrations of $Ag(MeCN)_4^+$, **b** is identical to **a** but only the two reduction processes are presented

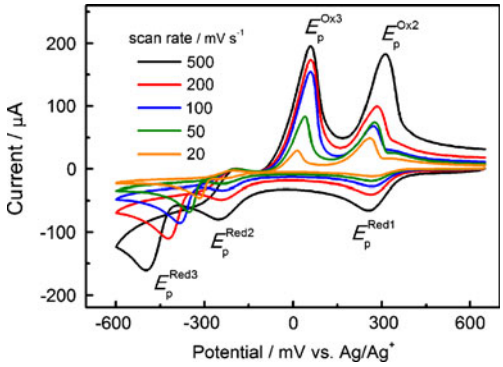

Fig. 9 Cyclic voltammograms for 1.0 mM $TCNQF_4$ and 2.0 mM $Ag(MeCN)_4^+$ in acetonitrile (0.1 M Bu_4NPF_6) obtained with a 3.0-mm diameter GC electrode at designated scan rates

Characterization of Ag-$TCNQF_4$ compounds by spectroscopic and microscopic techniques

Chemically synthesized AgTCNQF4

The single crystal X-ray structure of $AgTCNQF_4$ electrochemically synthesized by reduction of $TCNQF_4$ at an Ag electrode in acetonitrile at a constant current has been determined [13]. The $TCNQF_4^{1-}$ anions are nearly perfectly eclipsed with a high degree of dimerization, which results in this compound being essentially diamagnetic.

Here, $AgTCNQF_4$ was chemically synthesized as described in the section "Solubility of $AgTCNQF_4$ in acetonitrile", and characterized by UV-vis, FTIR, and Raman spectra as shown in Fig. 11. The UV-vis spectrum of $AgTCNQF_4$ dissolved in acetonitrile has three absorption bands with λ_{max} at 411, 686, and 752 nm (Fig. 11a), which is consistent with the presence of only $TCNQF_4^{1-}$ [29–31]. In solid-state, X-ray structure [13] shows that $TCNQF_4^{1-}$ is better represented as $(TCNQF_4)_2^{2-}$ dimer, although for convenience, sometimes referred to this species as $TCNQF_4^{1-}$. The IR bands for the solid material are at 2,221, 2,210, and 2,195 cm^{-1} (Fig. 11b) can be assigned to the C≡N stretch in the $(TCNQF_4)_2^{2-}$ dimer [13, 32] with the splitting being the result of coordination of $TCNQF_4^{1-}$ to the Ag^+ cation via the CN groups [33]. The locations of these bands are the same as those reported for $AgTCNQF_4$ in ref. [13] (i.e., 2,220, 2,213, and 2,197 cm^{-1}), within experimental error. The IR band at 1,501 cm^{-1} for $AgTCNQF_4$ is typical of the π(C=C) ring stretch and is usually found at higher energy than that for $TCNQF_4$ (1,493 cm^{-1}). The presence of this band also implies that the $TCNQF_4$ units in $AgTCNQF_4$ are present in the reduced form of $TCNQF_4^{1-}$ [13, 16, 32]. The C–F out of plane bending mode is located at 1,205 cm^{-1} [13, 17], shifted to higher energy by 15 cm^{-1} compared with $TCNQF_4$ (1,190 cm^{-1}). The Raman spectrum for the chemically synthesized solid $AgTCNQF_4$ exhibits three bands at

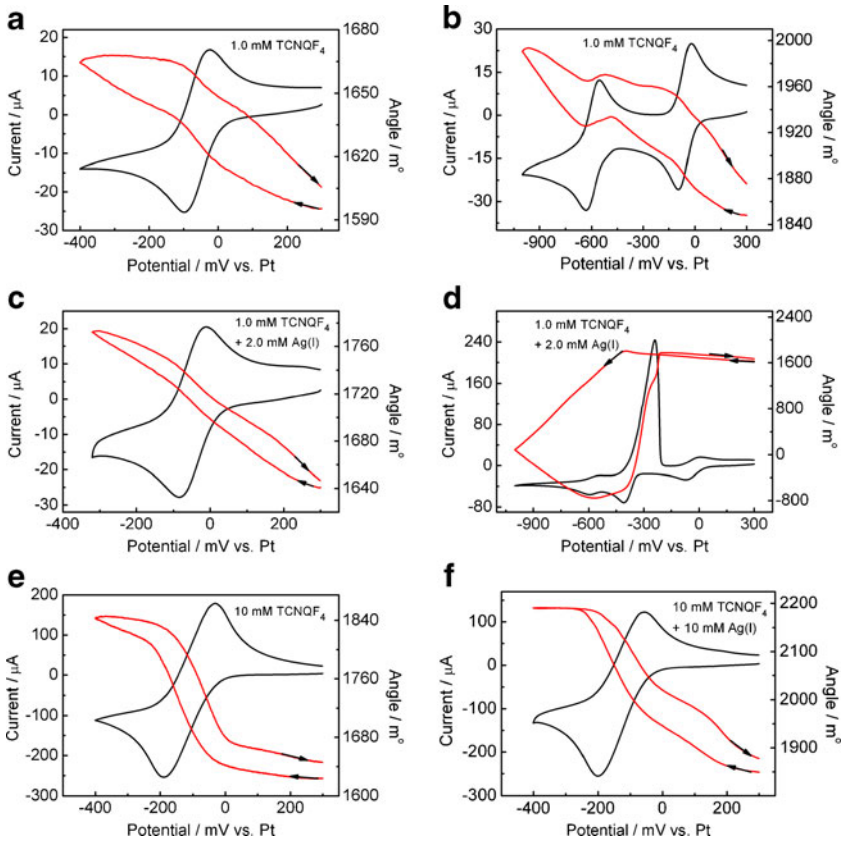

Fig. 10 In situ cyclic voltammetric (*black*) (scan rate= 100 mV s^{-1}) and SPR (*red*) data obtained on a gold electrode for **a**, **b** 1.0 mM $TCNQF_4$, **c**, **d** 1.0 mM $TCNQF_4$ and 2.0 mM $Ag(MeCN)_4^+$, **e** 10.0 mM $TCNQF_4$ and **f** 10.0 mM $TCNQF_4$, and 10.0 mM $Ag(MeCN)_4^+$ in acetonitrile (0.1 M Bu_4NPF_6)

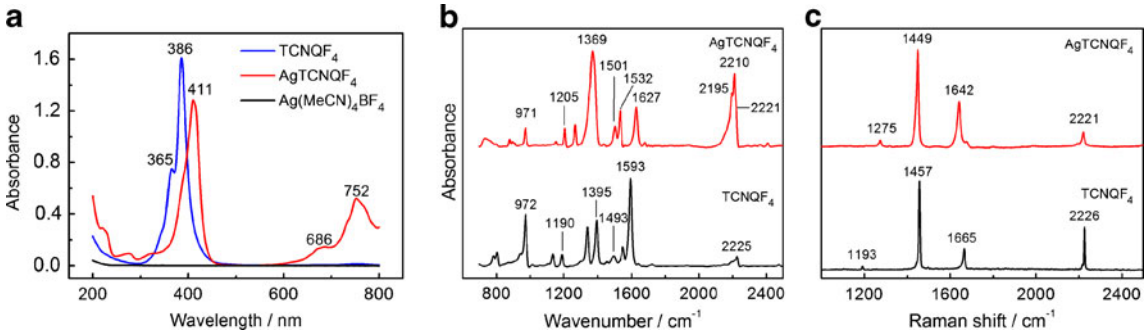

Fig. 11 Characterization of chemically synthesized $AgTCNQF_4$ by **a** UV-vis spectra (solution), **b** FTIR spectra (*solid*), **c** Raman spectra (*solid*) compared with $TCNQF_4$

2,221, 1,642, and 1,449 cm^{-1}, which respectively correspond to C≡N, C=C ring, and C–CN wing stretches [16, 17]. Compared with $TCNQF_4$ (2,226, 1,665, and 1,457 cm^{-1}), all three of these Raman vibration modes exhibit lower Raman shift as a result of the reduction of $TCNQF_4$ to $TCNQF_4^{1-}$ [16, 17]. A relative decrease in the intensity of the C≡N stretch band also is a spectroscopic fingerprint for the formation of $TCNQF_4^{1-}$ reduced form [17].

Electrochemically synthesized $AgTCNQF_4$

$AgTCNQF_4$ can be electrochemically synthesized and deposited on the surface of an electrode under conditions in which the solubility product of $AgTCNQF_4$ is exceeded. Hence, acetonitrile (0.1 M Bu_4NPF_6) solutions containing 2.0 mM $TCNQF_4$ and 10.0 mM $Ag(MeCN)_4^+$ were used to electrocrystallize $AgTCNQF_4$ onto an ITO electrode surface. A constant potential of 100 mV was applied to the ITO electrodes for 30 min to reduce $TCNQF_4$ to $TCNQF_4^{1-}$. The electrocrystallized material was rinsed with ethanol, dried under a nitrogen gas stream for 10 min, and then under vacuum for 5 h prior to characterization. An optical microscopic image shows that the morphology of the sample on ITO is needle-shaped with crystal lengths of ~200 μm (see Fig. 12a). UV-vis, FTIR, and Raman spectra for the electrochemically synthesized $AgTCNQF_4$ are identical to the chemically synthesized $AgTCNQF_4$ (see Fig. 11). It is likely that the $AgTCNQF_4$ samples chemically or electrochemically synthesized exist in the same phase. Interestingly, UV-vis, FTIR, and Raman spectra for $AgTCNQF_4$ electrochemically synthesized by reduction of immobilized solid $TCNQF_4$ on an ITO electrode surface placed in a 0.1 M $AgNO_3$ aqueous solution at a potential of 550 mV vs. Ag/AgCl are also the same as the chemically synthesized $AgTCNQF_4$, within experimental error. Figure 12b shows a SEM image for the $AgTCNQF_4$ electrochemically synthesized onto a GC electrode surface via solid–solid phase transformation under conditions described in Fig. 12b.

Chemically synthesized Ag_2TCNQF_4

Ag_2TCNQF_4 was chemically synthesized by mixing 2.0 mL of 5.0 mM $TCNQF_4^{2-}$ acetonitrile solution, which was prepared by exhaustive reductive electrolysis of 5.0 mM $TCNQF_4$ at a Pt foil electrode in acetonitrile (0.1 M Bu_4NPF_6) at −400 mV vs. Ag/Ag^+, with 2.0 mL of 10.0 mM $Ag(MeCN)_4BF_4$ in acetonitrile. A white precipitate of

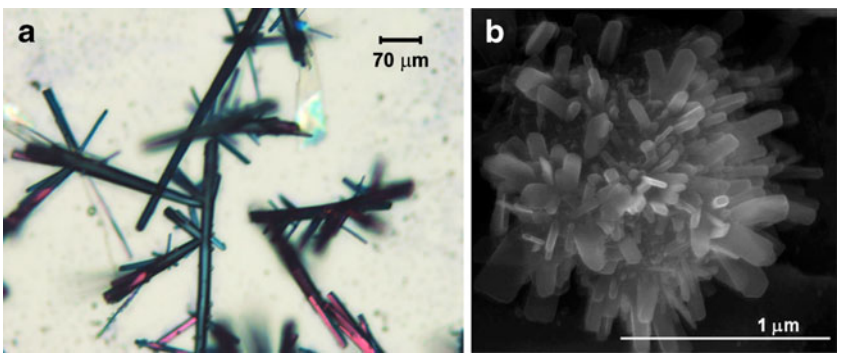

Fig. 12 **a** Optical microscopic image of $AgTCNQF_4$ electrocrystallized onto ITO electrode surface from acetonitrile (0.1 M Bu_4NPF_6) containing 2.0 mM $TCNQF_4$ and 10.0 mM $Ag(MeCN)_4^+$ by holding the potential at 100 mV for 30 min, **b** SEM image of $AgTCNQF_4$ electrochemically synthesized by reduction of solid $TCNQF_4$, which was physically immobilized on a GC electrode surface and placed in a 0.1 M $AgNO_3$ aqueous solution, at 550 mV vs. Ag/AgCl for 10 min

Ag_2TCNQF_4 formed immediately, but gradually changed to pale green within a few minutes. The color of the solution also turned green. The precipitate was collected by centrifugation and washed three times with acetonitrile before filtration to obtain the solid and solution. UV-vis spectroscopy reveals the presence of both $TCNQF_4^{1-}$ and $TCNQF_4^{2-}$ (a specific band for $TCNQF_4^{2-}$ [29] was observed with λ_{max} at 333 nm) in the filtered solution. The washed solid was dried under a stream of N_2 gas for 10 min and in vacuum for 1 h before being characterized by FTIR spectroscopy. Four IR bands associated with the C≡N stretch are observed at 2,212, 2,193 cm^{-1} (which accord with the presence of $TCNQF_4^{1-}$), 2,159 and 2,127 cm^{-1} (which are characteristics for $TCNQF_4^{2-}$ dianion [18, 29]). Apparently, the $TCNQF_4^{2-}$ dianion rapidly reacts with the Ag^+ cation in acetonitrile to form a white precipitate of Ag_2TCNQF_4. However, this solid is not thermodynamically stable and gradually decomposes via a redox reaction (Eq. 6) to produce $AgTCNQF_4$ and metallic Ag. This internal redox reaction is thermodynamically allowed since the potentials for the oxidation of $TCNQF_4^{2-}$ and reduction of $Ag(MeCN)_4^+$ in acetonitrile are very close (see section "Voltammetry of $TCNQF_4$ and $Ag(MeCN)_4^+$ in acetonitrile (0.1 M Bu_4NPF_6) solution"). However, on the voltammetric time scale (scan rate=20 mV s^{-1}), Ag_2TCNQF_4 can be formed on the electrode surface so that a stripping process associated with Ag_2TCNQF_4 is observed in the positive potential direction scan (see section "Cyclic voltammetry of $TCNQF_4$ in the presence of $Ag(MeCN)_4^+$ in acetonitrile (0.1 M Bu_4NPF_6)"). The transformation of Ag_2TCNQF_4 to metallic Ag and $AgTCNQF_4$ also was observed to be catalyzed when exposing a thin film of Ag_2TCNQF_4 to low-power visible laser radiation [12].

$$(m+n)Ag_2TCNQF_4 \rightarrow mAg_2TCNQF_4 + nAg + nAgTCNQF_4 \quad (6)$$

Conclusions

Electrocrystallization of the dark blue $AgTCNQF_4$ solid onto electrode surfaces can be achieved in acetonitrile containing $TCNQF_4$ and $Ag(MeCN)_4^+$, as confirmed by UV-vis, FTIR, and Raman spectra. The electrocrystallization of $AgTCNQF_4$ occurs via the two processes given in Eqs. 4a and 4b.

In the solid phase, $TCNQF_4^{1-}$ anions in $AgTCNQF_4$ exist in dimer form [13]. The potential for reduction of $Ag(MeCN)_4^+$ to Ag metal is much more negative than that for the $TCNQF_4^{0/1-}$ reduction process. Therefore, electrochemical synthesis of $AgTCNQF_4$ is easy to perform in acetonitrile via the above method without concern for overlap with reduction of $Ag(MeCN)_4^+$. However, electrocrystallization can only occur when the solubility product of $AgTCNQF_4$ is exceeded and if the kinetics of precipitation of $AgTCNQF_4$ is sufficiently fast. The solubility and solubility product of $AgTCNQF_4$ in acetonitrile in the presence or absence of 0.1 M Bu_4NPF_6 supporting electrolyte were determined to be $1.10\pm0.04\times10^{-3}$ M and $1.22\pm0.08\times10^{-6}$ M^2 or $7.08\pm0.16\times10^{-4}$ M and $5.01\pm0.22\times10^{-7}$ M^2, respectively, allowing conditions to be identified that allow $AgTCNQF_4$ to be electrocrystallized.

The reversible potentials for the $TCNQF_4^{0/1-}$ and $TCNQF_4^{1-/2-}$ reduction processes are almost independent of GC, Au, Pt, and ITO electrodes, while the peak potential for reduction of $Ag(MeCN)_4^+$ to metallic Ag is strongly dependent on electrode material. Comparing the potential for reduction of $TCNQF_4^{1-}$ to $TCNQF_4^{2-}$, the reduction of $Ag(MeCN)_4^+$ occurs about 200 mV more positive at a Au electrode, slightly more positive at a Pt electrode and a little more negative at GC and ITO electrodes. Therefore, electrochemical synthesis of bulk Ag_2TCNQF_4 on Au and Pt substrates is difficult, and even on GC and ITO electrodes because of the close proximity of potentials for reduction of $TCNQF_4^{1-}$ and $Ag(MeCN)_4^+$, but it can be formed transiently. Another complication in electrocrystallization of Ag_2TCNQF_4 is that this material is not stable and decomposes gradually through a redox reaction to generate $AgTCNQF_4$ and Ag. The presence of $AgTCNQF_4$ generated via the internal redox reaction in chemically synthesized Ag_2TCNQF_4 is detected via UV-vis and FTIR spectroscopy.

Optical microscopic image shows that the morphology of $AgTCNQF_4$ electrocrystallized onto ITO is needle-shaped. UV-vis, FTIR, and Raman spectra for $AgTCNQF_4$ electrochemically synthesized from $TCNQF_4$ and $Ag(MeCN)_4^+$ in acetonitrile, electrochemically synthesized $AgTCNQF_4$ from solid $TCNQF_4$ immobilized on an ITO electrode surface placed in 0.1 M $AgNO_3$ aqueous solution and chemically synthesized $AgTCNQF_4$ are spectroscopically indistinguishable. It seems that all the $AgTCNQF_4$ complexes exist in the same phase.

Acknowledgments Financial support from the Australian Research Council is greatly appreciated. T. H. L gratefully acknowledges graduate scholarship funding from Danang City in Vietnam and the award of a Monash University Faculty of Science Dean's International Postgraduate Research Scholarship.

References

1. Ballester L, Gutierrez A, Perpina MF, Azcondo MT (1999) Coord Chem Rev 190–192:447–470
2. Kuroda N, Sugimoto T, Hagiwara M, Hasanudin UK, Tada T, Uozaki H, Toyota N, Mogi I, Watanabe K, Motokawa M (2003) Synth Met 133–134:535–537
3. LeBlanc OH Jr (1965) J Chem Phys 42:4307–4308
4. Ueda K, Takahashi M, Tomizawa H, Miki E, Faulmann C (2005) J Mol Struct 751:12–16

5. Ran CB, Peng HL, Zhou W, Yu XC, Liu ZF (2005) J Phys Chem B 109:22486–22490
6. Peng HL, Ran CB, Yu XC, Zhang R, Liu ZF (2005) Adv Mater 17:459
7. Cano M, Palenzuela B, Rodriguez-Amaro R (2006) Electroanalysis 18:1068–1074
8. Llopis X, Merkoci A, del Valle M, Alegret S (2005) Sensor Actuator B Chem 107:742–748
9. Pandey PC, Upadhyay S, Sharma S (2003) Electroanalysis 15:1115–1119
10. Yasuda A, Seto J (1988) J Electroanal Chem 247:193–202
11. Valade L, De Caro D, Malfant I (2003) Thin films and nano-objects of molecule-based materials. Processing methods and application to materials exhibiting conductive, magnetic or photochrornic properties. Ouahab L, Yagubskii E (eds), Corfu, GREECE, pp. 241–268
12. Kotsiliou AM, Risen WM (1988) Solid State Commun 68:503–505
13. O'Kane SA, Clerac R, Zhao HH, Xiang OY, Galan-Mascaros JR, Heintz R, Dunbar KR (2000) J Solid State Chem 152:159–173
14. Hibbs W, Arif AM, Botoshansky M, Kaftory M, Miller JS (2003) Inorg Chem 42:2311–2322
15. Sugano T, Fukasawa T, Kinoshita M (1990) Magnetic-interactions among unpaired electrons in charge-transfer complexes of organic donors having a neutral radical. Tubingen, Fed Rep Ger, pp. 3281–3284
16. Xiao K, Rondinone AJ, Puretzky AA, Ivanov IN, Retterer ST, Geohegan DB (2009) Chem Mater 21:4275–4281
17. Ouyang CB, Guo YB, Liu HB, Zhao YJ, Li GX, Li YJ, Song YL, Li YL (2009) J Phys Chem C 113:7044–7051
18. Lopez N, Zhao HH, Prosvirin AV, Chouai A, Shatruk M, Dunbar KR (2007) Chem. Commun.:4611–4613
19. Lopez N, Zhao HH, Prosvirin AV, Wernsdorfer W, Dunbar KR (2010) Dalton Trans 39:4341–4352
20. Potember RS, Poehler TO, Rappa A, Cowan DO, Bloch AN (1982) Synth Met 4:371–380
21. Harris AR, Neufeld AK, O'Mullane AP, Bond AM (2006) J Mater Chem 16:4397–4406
22. Harris AR, Neufeld AK, O'Mullane AP, Bond AM, Morrison RJS (2005) J Electrochem Soc 152:C577–C583
23. Harris AR, Nafady A, O'Mullane AP, Bond AM (2007) Chem Mater 19:5499–5509
24. Wheland RC, Gillson JL (1976) J Am Chem Soc 98:3916–3925
25. Bard AJ, Faulkner LR (2001) Electrochemical methods: fundamentals and applications. Wiley, New York
26. Bond AM, Fletcher S, Marken F, Shaw SJ, Symons PG (1996) J Chem Soc Faraday Trans 92:3925–3933
27. Bond AM, Symons PG, Fletcher S (1998) Analyst (Cambridge, United Kingdom) 123:1891–1904
28. Fletcher S, Halliday CS, Gates D, Westcott M, Lwin T, Nelson G (1983) J Electroanal Chem 159:267–285
29. Dixon DA, Calabrese JC, Miller JS (1989) J Phys Chem 93:2284–2291
30. Zanon I, Pecile C (1983) J Phys Chem 87:3657–3664
31. Maity AN, Sarkar B, Niemeyer M, Sieger M, Duboc C, Zalis S, Kaim W (2008) Dalton Trans.:5749–5753
32. Azcondo MT, Ballester L, Golhen S, Gutierrez A, Ouahab L, Yartsev S, Delhaes P (1999) J Mater Chem 9:1237–1244
33. Long G, Willett RD (2001) Inorganica Chimica Acta 313:1–14